



Impact of Material and Architecture Model Parameters on the Failure of Woven Ceramic Matrix Composites (CMCs) Via the Multiscale Generalized Method of Cells

Kuang C. Liu
Arizona State University, Tempe, Arizona

Steven M. Arnold
Glenn Research Center, Cleveland, Ohio

NASA STI Program . . . in Profile

Since its founding, NASA has been dedicated to the advancement of aeronautics and space science. The NASA Scientific and Technical Information (STI) program plays a key part in helping NASA maintain this important role.

The NASA STI Program operates under the auspices of the Agency Chief Information Officer. It collects, organizes, provides for archiving, and disseminates NASA's STI. The NASA STI program provides access to the NASA Aeronautics and Space Database and its public interface, the NASA Technical Reports Server, thus providing one of the largest collections of aeronautical and space science STI in the world. Results are published in both non-NASA channels and by NASA in the NASA STI Report Series, which includes the following report types:

- **TECHNICAL PUBLICATION.** Reports of completed research or a major significant phase of research that present the results of NASA programs and include extensive data or theoretical analysis. Includes compilations of significant scientific and technical data and information deemed to be of continuing reference value. NASA counterpart of peer-reviewed formal professional papers but has less stringent limitations on manuscript length and extent of graphic presentations.
- **TECHNICAL MEMORANDUM.** Scientific and technical findings that are preliminary or of specialized interest, e.g., quick release reports, working papers, and bibliographies that contain minimal annotation. Does not contain extensive analysis.
- **CONTRACTOR REPORT.** Scientific and technical findings by NASA-sponsored contractors and grantees.

- **CONFERENCE PUBLICATION.** Collected papers from scientific and technical conferences, symposia, seminars, or other meetings sponsored or cosponsored by NASA.
- **SPECIAL PUBLICATION.** Scientific, technical, or historical information from NASA programs, projects, and missions, often concerned with subjects having substantial public interest.
- **TECHNICAL TRANSLATION.** English-language translations of foreign scientific and technical material pertinent to NASA's mission.

Specialized services also include creating custom thesauri, building customized databases, organizing and publishing research results.

For more information about the NASA STI program, see the following:

- Access the NASA STI program home page at <http://www.sti.nasa.gov>
- E-mail your question via the Internet to help@sti.nasa.gov
- Fax your question to the NASA STI Help Desk at 443-757-5803
- Telephone the NASA STI Help Desk at 443-757-5802
- Write to:
NASA Center for AeroSpace Information (CASI)
7115 Standard Drive
Hanover, MD 21076-1320



Impact of Material and Architecture Model Parameters on the Failure of Woven Ceramic Matrix Composites (CMCs) Via the Multiscale Generalized Method of Cells

Kuang C. Liu
Arizona State University, Tempe, Arizona

Steven M. Arnold
Glenn Research Center, Cleveland, Ohio

Prepared for the
35th International Conference and Exposition on Advanced Ceramics and Composites (ICACC '11)
sponsored by the American Ceramic Society
Daytona Beach, Florida, January 23–28, 2011

National Aeronautics and
Space Administration

Glenn Research Center
Cleveland, Ohio 44135

Trade names and trademarks are used in this report for identification only. Their usage does not constitute an official endorsement, either expressed or implied, by the National Aeronautics and Space Administration.

Level of Review: This material has been technically reviewed by technical management.

Available from

NASA Center for Aerospace Information
7115 Standard Drive
Hanover, MD 21076-1320

National Technical Information Service
5301 Shawnee Road
Alexandria, VA 22312

Available electronically at <http://www.sti.nasa.gov>

Impact of Material and Architecture Model Parameters on the Failure of Woven Ceramic Matrix Composites (CMCs) Via the Multiscale Generalized Method of Cells

Kuang C. Liu
Arizona State University
Tempe, Arizona 85287

Steven M. Arnold
National Aeronautics and Space Administration
Glenn Research Center
Cleveland, Ohio 44135

Abstract

It is well known that failure of a material is a locally driven event. In the case of ceramic matrix composites (CMCs), significant variations in the microstructure of the composite exist and their significance on both deformation and life response need to be assessed. Examples of these variations include changes in the fiber tow shape, tow shifting/nesting and voids within and between tows. In the present work, the effects of many of these architectural parameters and material scatter of woven ceramic composite properties at the macroscale (woven RUC) will be studied to assess their sensitivity. The recently developed Multiscale Generalized Method of Cells methodology is used to determine the overall deformation response, proportional elastic limit (first matrix cracking), and failure under tensile loading conditions. The macroscale responses investigated illustrate the effect of architectural and material parameters on a single RUC representing a five harness satin weave fabric. Results shows that the most critical architectural parameter is weave void shape and content with other parameters being less in severity. Variation of the matrix material properties was also studied to illustrate the influence of the material variability on the overall features of the composite stress-strain response.

Introduction

Multiscale modeling has been applied to both laminated and woven composites in the past. Although nomenclature in the literature varies, typically a multiscale modeling analysis will follow length scales shown in Figure 1 for continuum modeling. These scales, progressing from left to right in Figure 1, are the microscale (constituent level; fiber, matrix, interface), the mesoscale (tow), the macroscale (repeating woven unit cell), and the global/structural scale. Traditionally, one traverses (transcends (moves right) or descends (moves left)) these scales via homogenization and localization techniques, respectively (Figure 1 and Figure 2(a)); where a homogenization technique provides the properties or response of a “**structure**” (higher level) given the properties or response of the structure’s “**constituents**” (lower scale). Conversely, localization techniques provide the response of the constituents given the response of the structure. Figure 2(b) illustrates the interaction of homogenization and localization techniques, in that during a multiscale analysis, a particular stage in the analysis procedure can function on both levels simultaneously. For example, during the process of homogenizing the stages represented by X and Y to obtain properties for the stage represented by V, X and Y should be viewed as the constituent level while V is on the structure level. However, during the process of homogenizing V and W to obtain properties for U, V is now on the constituent level (as is W). Obviously, the ability to homogenize and localize accurately requires a sophisticated theory that relates the geometric and material characteristics of structure and constituents.

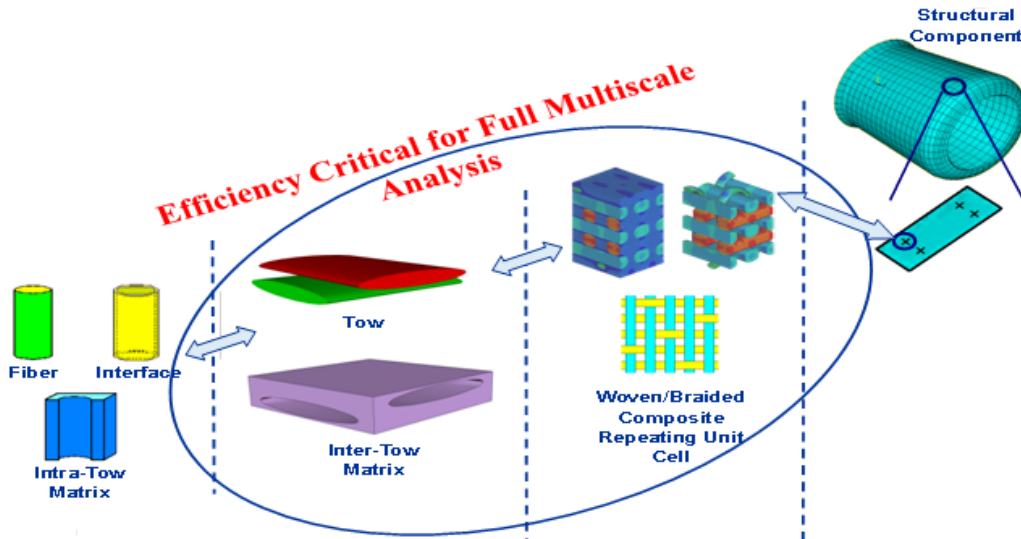


Figure 1.—Illustration of associated levels scales for woven/braided composite analysis.

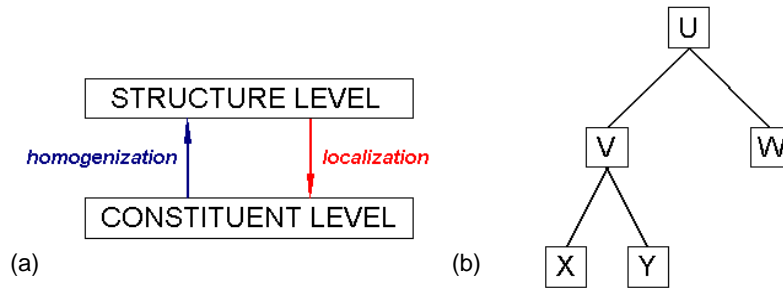


Figure 2.—(a) Homogenization provides the ability to determine structure level properties from constituent level properties while localization provides the ability to determine constituent level responses from structure level results. (b) Example tree diagram.

With the recent development of the MultiScale Generalized Method of Cells (MSGMC), one can now ascertain the influence of architectural parameters, such as volume fraction, weave geometry, tow geometry, etc., at each associated length scale, for composites; particularly woven and braided composites. This enables the determination of which effect/parameter, at a given length scale, is impactful/relevant at higher length scales. For example, matrix elastic modulus is a microscale effect, changing this value will have a direct effect at the next largest length scale (e.g., mesoscale), but its effect at the macro or structural scale cannot necessarily be assumed. Similarly the tow fiber volume fraction, which is a mesoscale effect, should have a direct impact on the response at the macroscale, yet its effect at the global scale is difficult to deduce *a priori*. Furthermore, experimental investigations have shown that in typical composite (particularly woven) materials there exist significant variations in the meso and macroscale architectural features. Yet most analyses performed (until now) assume an idealized or pristine material and architecture at every length scale. Such an assumption was required, up until now, to avoid the computationally exhaustive multiscale modeling of every minute variation in architecture at every length scale, via the finite element method. The objective of this paper is to perform a preliminarily

yet truly multiscale¹ investigation to study lower length scale effects and determine their significance at the macro and structural scale.

Multiscale Generalized Method of Cells

Overview

Analysis of woven fabric composites can be generalized into several relevant length scales (from largest to smallest): macro, meso, and micro. The macroscale weave refers to the RUC of the weave, for a five-harness satin fabric, see Figure 3. The mesoscale refers to an RUC of the fiber tow; wherein this RUC represents a bundle of fibers (typically 700 to 1000 for ceramic matrix composites) with a given packing arrangement. The smallest length scale is the microscale, which represents the fundamental constituent materials, such as the monofilament fiber, interphase and matrix itself.

This multiscale analysis uses the recently developed MSGMC methodology (Ref. 1). At the macroscale, each fabric composite (e.g., plain or 5HS, see Figure 3) was discretized into $N_\alpha \times N_\beta \times N_\gamma$ subcells using the assumption of triple periodicity; wherein, for example, a subcell used to represent a fiber tow is further idealized at the mesoscale by $N_{\{\alpha\beta\gamma\}\beta} \times N_{\{\alpha\beta\gamma\}\gamma}$ subcells using the assumption of double periodicity, wherein each of these subcells are represented by the constitutive properties of either a fiber or matrix at the microscale. This recursive methodology (wherein the generalized method of cells (GMC), see Paley and Aboudi (Ref. 2) and Aboudi (Ref. 3), is called within GMC) is shown in Figure 4, and can be accounted for by attaching the superscript $\{\alpha\beta\gamma\}$ to each. There are several architectural parameters at the meso, macro, and structural level required to fully define the discretized subcell geometries. At the mesoscale, both tow volume fraction and tow packing are required, while at the macroscale, weave architecture, weave volume fraction, tow aspect ratio and ply nesting are required. Furthermore, at the structural level although not addressed in this paper, the spatial distribution of the macroscale RUCs are required, i.e., uniform—each subcell is associated with the same macroscale RUC or random—subcells are associated with a uniform distribution of macroscale RUCs. It has been of recent interest to study the effects of these parameters and understand what the driving factors are for both elastic and inelastic response, see Reference 4.

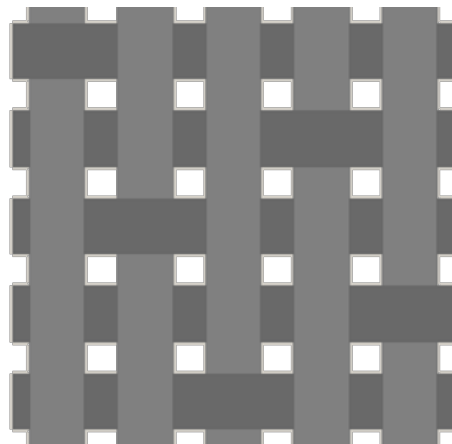


Figure 3.—Five harness satin macroscale RUC.

¹Here the term multiscale refers to an analysis in which at least three levels of scales are accounted for, wherein at least two homogenizations/localizations are required.

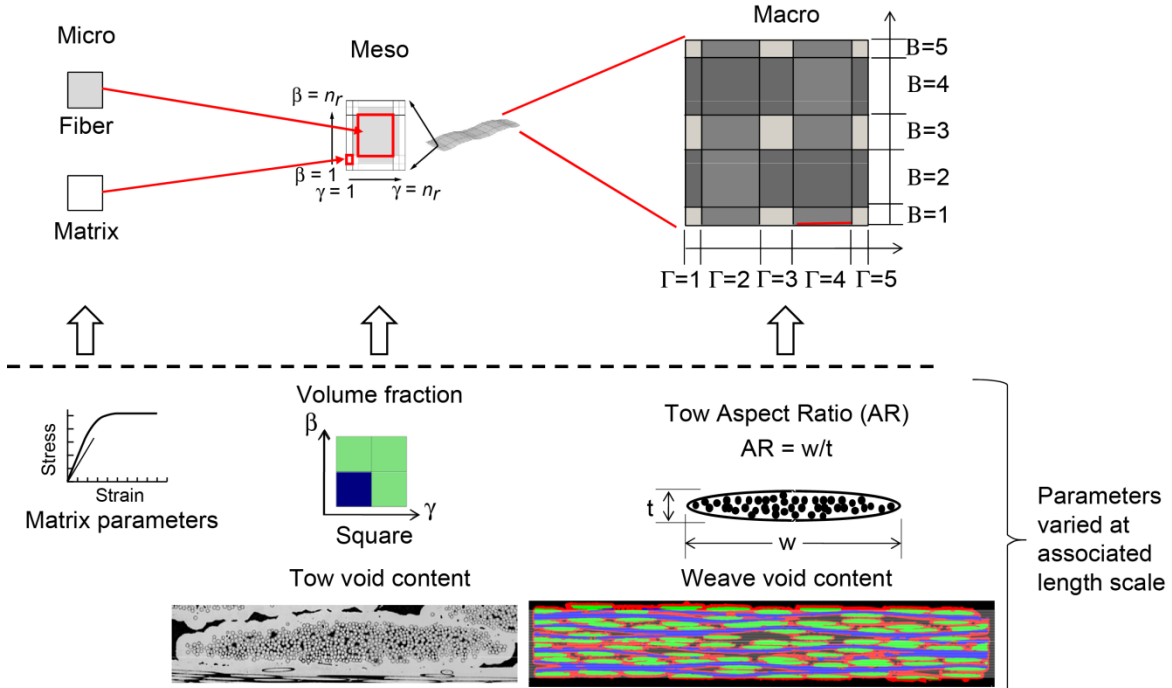


Figure 4.—Multiscale methodology with architectural effects being varied shown at three length scales considered. Actual micrographs are complements of P. Bonacuse, NASA Glenn, 2010.

Microscale (Constitutive Modeling)

The MSGMC is used to represent the woven fabric composite starting with its constituent materials, i.e., the fiber (monofilament), coating (interphase) and matrix and progress up the various length scales. The microscale is the only length scale where explicit constitutive models are applied to the various phases (e.g., fiber and matrix). Stress states and tangent moduli for larger length scales are determined through the Generalized Method of Cells (GMC) triply-periodic homogenization procedure developed by Aboudi (Ref. 3). The monofilament fibers are modeled using a linear elastic relationship, i.e., Hooke's Law, and the matrix material is represented by a scalar damage mechanics type relationship based on a tangent modulus relationship. Details for the damage model can be found in the following sections. Although, ceramics are typically stochastic herein all microscale constituent parameters (i.e., modulus, failure strength, etc.) were assumed to be *deterministic* in this analysis. The stresses in any subcell in the microscale can be determined from the following equation. The stiffness $C^{\{\alpha\beta\gamma\}\{\beta\gamma\}}$ is determined from the given material parameters and modified by a scalar damage measure $\lambda^{\{\alpha\beta\gamma\}\{\beta\gamma\}}$ and the strains $\varepsilon^{\{\alpha\beta\gamma\}\{\beta\gamma\}}$ are determined from localization from the mesoscale. This is possible through a concentration matrix, A , determined by GMC, which is a function of the subcell geometry and stiffness matrix.

$$\sigma^{\{\alpha\beta\gamma\}\{\beta\gamma\}} = \left(\lambda^{\{\alpha\beta\gamma\}\{\beta\gamma\}} \right) C^{\{\alpha\beta\gamma\}\{\beta\gamma\}} \varepsilon^{\{\alpha\beta\gamma\}\{\beta\gamma\}} \quad (1)$$

$$\varepsilon^{\{\alpha\beta\gamma\}\{\beta\gamma\}} = A^{\{\alpha\beta\gamma\}\{\beta\gamma\}} \varepsilon^{\{\alpha\beta\gamma\}} \quad (2)$$

Mesoscale (Tow)

The mesoscale is used to represent the periodic structure of a fiber tow. At the mesoscale, there are two significant architectural parameters: fiber packing and tow volume fraction. Both of these parameters govern the mesoscale subcell geometries. The response of the mesoscale is subject to these parameters as

well as the material variation at the microscale. The continuous fiber tows are assumed to be represented by a doubly-periodic RUC of dimensions $h_{\{\alpha\beta\gamma\}} \times l_{\{\alpha\beta\gamma\}}$ consisting of constituents from the microscale, this assumption is confirmed by the tow micrograph shown in Figure 4. An example of such an RUC discretized for GMC is shown in Figure 4, where the inner region (shown in grey) denotes the fiber tow and the outer region (shown in white) is the matrix. The RUC is discretized in such a manner that it is composed of $N_{\{\alpha\beta\gamma\}\beta} \times N_{\{\alpha\beta\gamma\}\gamma}$ rectangular subcells, with each subcell having dimensions $h_{\{\alpha\beta\gamma\}\beta} \times l_{\{\alpha\beta\gamma\}\gamma}$. From this point forward, superscripts with lowercase Greek letters denote a specific subcell at the microscale, superscripts of uppercase Greek letters denote a specific subcell at the macroscale and superscripts with lowercase Roman letters denotes macroscale variables. Fiber tow packing and volume fraction typically govern the architecture of the mesoscale RUC but must be in accordance with the previously described RUC microstructural parameters. The resulting stress in the fiber tow can be determined from the GMC homogenization process, where in GMC, the current stress and current tangent moduli of a particular fiber tow at a point are determined through a volume averaging integral over the repeating unit cell. This process is represented by the summation in the following equations, producing the first homogenization in the multiscale modeling framework. In these equations, σ denotes the Cauchy true stress, A denotes the strain concentration matrix, and C denotes the stiffness matrix (Refs. 2 and 3). The microscale subcell stresses and tangent moduli needed to complete the summation are determined through the applied constitutive models for each constituent based on their current strain state. The mesoscale strains, which are used as the boundary conditions for the GMC analysis, are determined from the through thickness (tt) homogenization at the macroscale (done on a group by group basis, see Figure 6). The subscripts tt in the concentration matrix in Equation (5) denote the second portion of the two step homogenization process discussed later.

$$\sigma^{\{\alpha\beta\gamma\}} = \frac{1}{h_{\{\alpha\beta\gamma\}} l_{\{\alpha\beta\gamma\}}} \sum_{\{\alpha\beta\gamma\}\beta=1}^{N_{\{\alpha\beta\gamma\}\beta}} \sum_{\{\alpha\beta\gamma\}\gamma=1}^{N_{\{\alpha\beta\gamma\}\gamma}} \sigma^{\{\alpha\beta\gamma\}\{\beta\gamma\}} h_{\{\alpha\beta\gamma\}\beta} l_{\{\alpha\beta\gamma\}\gamma} \quad (3)$$

$$C^{\{\alpha\beta\gamma\}} = \frac{1}{h_{\{\alpha\beta\gamma\}} l_{\{\alpha\beta\gamma\}}} \sum_{\{\alpha\beta\gamma\}\beta=1}^{N_{\{\alpha\beta\gamma\}\beta}} \sum_{\{\alpha\beta\gamma\}\gamma=1}^{N_{\{\alpha\beta\gamma\}\gamma}} \lambda^{\{\beta\gamma\}} C^{\{\alpha\beta\gamma\}\{\beta\gamma\}} A^{\{\alpha\beta\gamma\}\{\beta\gamma\}} h_{\{\alpha\beta\gamma\}\beta} l_{\{\alpha\beta\gamma\}\gamma} \quad (4)$$

$$\varepsilon^{\{\alpha\beta\gamma\}} = A_{tt}^{\{\alpha\beta\gamma\}} A_{ip}^{\{\beta\gamma\}} \varepsilon \quad (5)$$

$$\sigma^{\{\alpha\beta\gamma\}} = C^{\{\alpha\beta\gamma\}} \varepsilon^{\{\alpha\beta\gamma\}} \quad (6)$$

Macroscale (Weave)

At the macroscale the RUC for the weave fabric is modeled. At this scale, the architecture is governed by the overall volume fraction, tow geometry (aspect ratio, width and thickness, and spacing within and between plies), void content and overall fabric thickness, wherein the subcell “constituent” response is obviously dependent on the mesoscale and microscale responses. The weave requires a triply-periodic RUC representation of size $d \times h \times l$ and discretized into $N_\alpha \times N_\beta \times N_\gamma$ parallelepiped subcells, with each subcell having dimensions $d_\alpha \times h_\beta \times l_\gamma$. At this length scale, a two step homogenization procedure was employed to determine the stiffness and macroscale stresses. This is to overcome the lack of normal and shear coupling inherent to the GMC formulation (Ref. 5). The first step involves a through thickness homogenization and the second step is an in-plane homogenization, where subscripts tt and ip denote

through thickness and in-plane respectively. Details for the subcell geometry and RUC information can be found in References 5 and 6.

Through thickness homogenization

$$\sigma^{\{\beta\gamma\}} = \frac{1}{d} \sum_{\alpha=1}^{N_{\alpha}} \sigma^{\{\alpha\beta\gamma\}} d_{\alpha} \tag{7}$$

$$C^{\{\beta\gamma\}} = \frac{1}{d} \sum_{\alpha=1}^{N_{\alpha}} A_{ii}^{\{\alpha\beta\gamma\}} C^{\{\alpha\beta\gamma\}} d_{\alpha} \tag{8}$$

$$\varepsilon^{\{\beta\gamma\}} = A_{ip}^{\{\beta\gamma\}} \varepsilon \tag{9}$$

$$\sigma^{\{\beta\gamma\}} = C^{\{\beta\gamma\}} \varepsilon^{\{\beta\gamma\}} \tag{10}$$

In-plane homogenization

$$\sigma = \frac{1}{hl} \sum_{\beta=1}^{N_{\beta}} \sum_{\gamma=1}^{N_{\gamma}} \sigma^{\{\alpha\beta\gamma\}} h_{\beta} l_{\gamma} \tag{11}$$

$$C = \frac{1}{hl} \sum_{\beta=1}^{N_{\beta}} \sum_{\gamma=1}^{N_{\gamma}} A_{ip}^{\{\beta\gamma\}} C^{\{\beta\gamma\}} h_{\beta} l_{\gamma} \tag{12}$$

$$\sigma = C \varepsilon \tag{13}$$

**Modeling Ceramic Matrix Composites With MSGMC
Weave Repeating Unit Cell**

For this particular study, a five harness satin weave is considered. In this idealization of the architecture, the repeating unit cell is assumed to be representative of the entire structure. A picture of the fabric with the repeating unit cell outlined in red is shown in Figure 5; in this study nesting/ply shifting will be ignored. To create a RUC suitable for analysis, the weave is discretized into several subvolume cells. There are two types of materials comprising all the subcells: fiber tows and interweave matrix. This final 3-D discretization is shown in Figure 6, along with example lower scale RUC representing the multiscale analyses of the interweave voids, tows and intra-tow voids. In the figure, fiber tows are indicated through the lined subcells. The lines indicate the direction of orientation. The blank subcells represent the interweave matrix. This results in a 10 by 10 by 4 sized RUC of dimensions shown in Equation (14). In this equation w

is the tow width and delta, δ , can be determined from $V_f = \frac{w}{(w + \delta)} V_{f_{tow}}$. The proper overall fiber volume

fraction and tow width is enforced by back calculating the tow spacing. Due to the chemical vapor infiltration process used to manufacture the woven fabric composites, there exists high levels of porosity, as shown in Figure 4, that cannot be neglected.

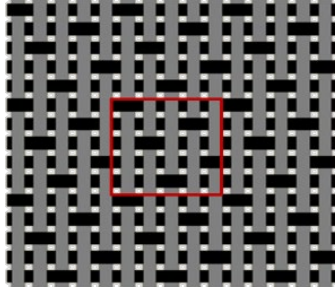


Figure 5.—Five harness satin repeating unit cell.

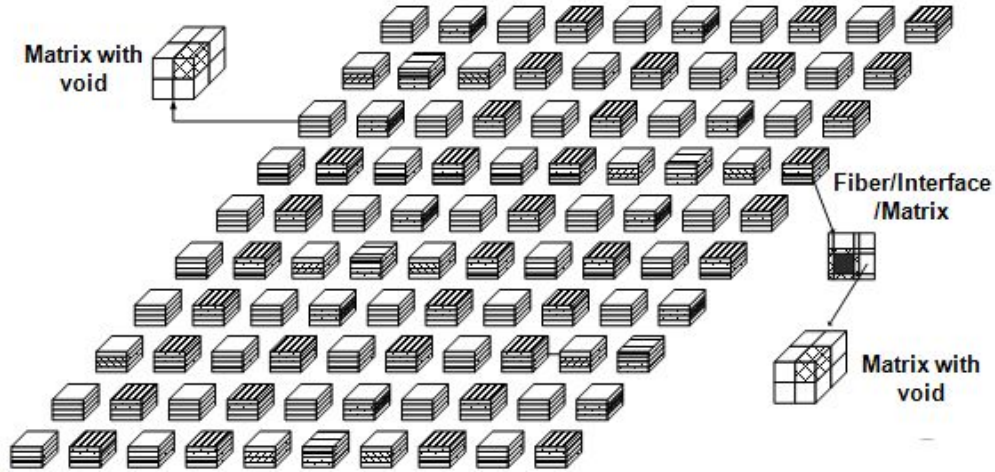


Figure 6.—Discretized five-harness satin subcell configuration.

Voids are accounted for in the RUC in one of three ways: 1) void content is neglected; 2) voids are assumed to be evenly distributed through the weave; or 3) voids are localized to critical areas determined from optical inspection (microscopy).

Figure 7 illustrates the three types of void modeling at the macroscale. The first figure shows no voids accounted for anywhere, the second figure depicts voids evenly distributed in the weave matrix (yellow, e.g., 12.7 percent void fraction), and the third figure shows high density (e.g., 85 percent) void regions in red and low density (e.g., 5 percent) void regions in blue. Note in both void idealization the total interweave void volume fraction is held constant at 12.7 percent. The voids are accounted for at a smaller length scale by analyzing a separate RUC homogenizing those properties. This is done for two primary reasons. First, explicit modeling of voids in GMC will tend to “eliminate” an entire row and column due to the constant strain field assumptions within a subcell. Yet, by performing a separate analysis, this effect is dampened since void volume and shape merely change the resulting anisotropic “constituent” response. Secondly, this allows for a faster, more accurate representation of void shape and distribution than explicitly modeling voids at this length scale.

$$\begin{aligned}
 D &= \{t/4, t/4, t/4, t/4\} \\
 H &= \{\delta, w, \delta, w, \delta, w, \delta, w\} \\
 L &= \{\delta, w, \delta, w, \delta, w, \delta, w\}
 \end{aligned}
 \tag{1}$$

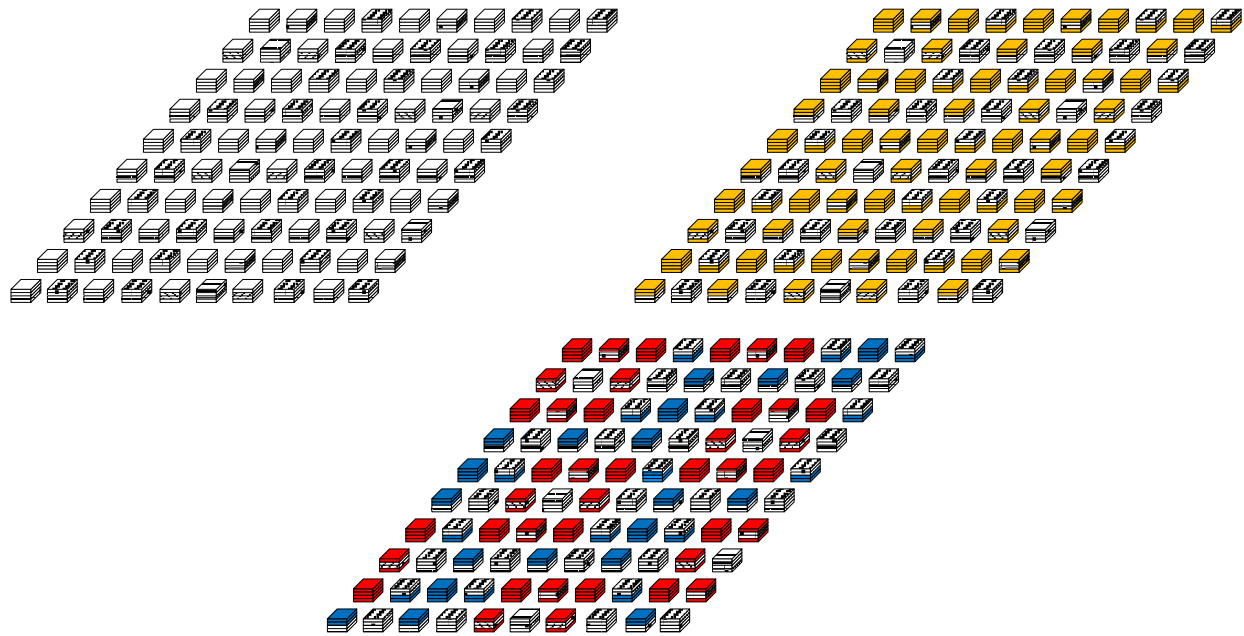


Figure 7.—Three types of void distributions; white no voids, yellow and blue represent 5 percent voids, and red represents 85 percent void content

Tow Repeating Unit Cell

The fiber tow bundles are modeled using a doubly periodic (continuously reinforced) 4 by 4 repeating unit cell consisting of three materials: fiber, fiber coating/interface, and matrix. Consequently the effective tow properties are influenced at each load step by all three constituents. In Figure 8, the black denotes the fiber, the hatched area represents the interphase, and white represents the matrix. At this level there are also voids due to the CVI process. However, the voids at this level appear to be more evenly distributed than at the weave level and thus are represented by evenly distributing the void content in the tow areas (see tow insert in Figure 4). This is accomplished once again by calling a separate void analysis for each matrix subcell in the RUC, just as described in the weave RUC section. Consequently, the effective tow properties are being influenced at each increment by all three constituents, matrix damage and intra-tow void volume fraction. For each fiber tow bundle, the orientation is carefully computed such that the undulation is properly accounted for and the failure criteria can be applied in the local coordinate system. Note no damage or failure of the interphase material will be accounted for in this study, since the BN coating’s stiffness is already approximately 20 times more compliant than the other two phases (see Table 1), thus minimizing its load carrying ability from the start.

Void Modeling

Voids are modeled through computation of a triply periodic (discontinuously reinforced) 2 by 2 by 2 RUC as shown in Figure 9. The hatched subcell represents the void portion while the white represents the matrix. The relative size of the void cell is what determines the overall void content in both the fiber tow bundles and the weave. As mentioned previously, modeling of voids as a separate GMC analysis has many advantages. The overall RUC of the weave will remain constant regardless of the shape and distribution of the voids, i.e., no rediscrization is required. Consequently, the void location, quantity, and geometry can be quickly changed. Lastly, the strength and stiffness degradations and stress concentrations can be captured through GMC without reducing the accuracy of the analysis at the macroscale.

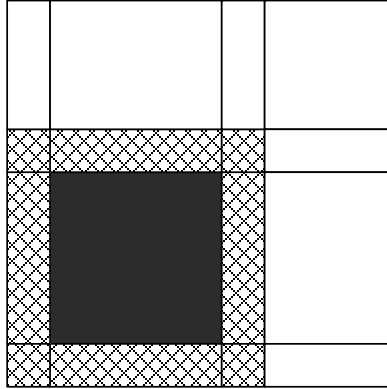


Figure 8.—Fiber tow bundle RUC.

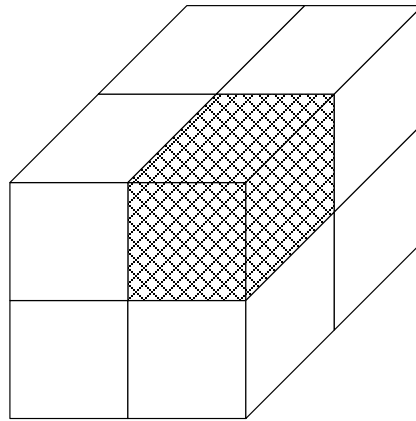


Figure 9.—Three dimensional void RUC.

Constitutive and Failure Modeling

Matrix Damage Modeling

The matrix material, assumed to be the same in both the weave and tow, is modeled through a scalar damage mechanics constitutive model driven by the magnitude of triaxiality, i.e., the first invariant of the stress/strain tensor. This constitutive model represents the cracks and brittle failure often seen in these CMCs. A scalar damage variable, ϕ , which varies between zero (no damage) and one (complete failure/damage), scales the elastic portion of the stiffness tensor and is employed directly in the stress strain relationship, shown in Equation (15).

$$\sigma = (1 - \phi)C\varepsilon \quad (14)$$

To determine the magnitude of damage, a damage rule is defined as

$$f = 3\varepsilon_H nK - \sigma_H = 0 \quad (15)$$

In this potential, n represents the damaged normalized secant modulus and K represents the instantaneous tangent bulk modulus, see Figure 10. This potential uses a stress and strain measure as defined by the first invariant of the respective tensors. This is shown in the following equations.

$$\begin{aligned}\sigma_H &= I_1(\sigma) = \frac{(\sigma_{11} + \sigma_{22} + \sigma_{33})}{3} \\ \varepsilon_H &= I_1(\varepsilon) = \frac{(\varepsilon_{11} + \varepsilon_{22} + \varepsilon_{33})}{3}\end{aligned}\tag{16}$$

The damage rule in (16) is only active once a critical stress criteria has been reach, i.e., it is only valid when $\sigma_H > \sigma_{\text{dam}}$. Equation (15) can be rewritten in incremental form with $i+1$ denoting the next increment ($\varepsilon^{i+1} = \varepsilon^i + \Delta\varepsilon^{i+1}$).

$$f = n3K^i\Delta\varepsilon_H^{i+1} - \Delta\sigma_H^{i+1} = 0\tag{17}$$

This can be converted to a strain based function by substituting the following relationship in for the stress increment

$$\Delta\sigma_H^{i+1} = 3\left(K^{i+1}\Delta\varepsilon_H^{i+1} + (K^{i+1} - K^i)\varepsilon_H^{i+1}\right)\tag{18}$$

Resulting in

$$nK^0\Delta\varepsilon_H^{i+1} - \left(K^{i+1}\Delta\varepsilon_H^{i+1} + (K^{i+1} - K^i)\varepsilon_H^{i+1}\right) = 0\tag{19}$$

where K^0 represents the initial bulk modulus, see Figure 10. The instantaneous tangent bulk modulus can be related back to the damage scalar through

$$K^{i+1} = (1 - \phi^{i+1})K^0\tag{20}$$

Substitution of (21) into (20) and simplification yields a formulation for the damage scalar.

$$1 - \phi^{i+1} = \lambda^{i+1} = \frac{n\Delta\varepsilon_H^{i+1} + \lambda^i\varepsilon_H^{i+1}}{(\Delta\varepsilon_H^{i+1} + \varepsilon_H^{i+1})}\tag{21}$$

where the initial value, ϕ^0 , is zero.

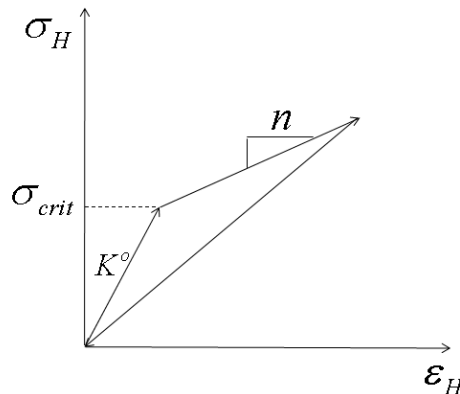


Figure 10.—Schematic showing bulk moduli change as function of triaxial strain.

Fiber Failure Modeling

The fiber is assumed to behave linearly elastic up to failure, with failure following the Hashin type failure criterion put forth in 1980, see Reference 7. This criterion determines the catastrophic failure of the fiber based on the axial and shear strengths. When the failure criterion exceeds 1, the fiber stiffness matrix is degraded to a minimal value. A key assumption made in this analysis is that the compliant fiber interface will fail simultaneously with the fiber and does not present its own failure modes. The failure stress levels presented later are an in-situ failure stress considering the interface.

$$f = \frac{\sigma_{11}^2}{\sigma_{axial}^2} + \frac{1}{\tau_{axial}^2} (\sigma_{13}^2 + \sigma_{12}^2) \quad (22)$$

Results

Problem Description

For this study, a five harness satin weave with a CVI-SiC matrix and iBN-Sylramic fiber (silicon carbide fiber coated with boron nitride) were chosen, due to the availability of experimental data for correlation. An approximate overall fiber volume fraction of 36 percent (which was held fixed for all cases examined) was determined along with a tow width of 1.25 mm and total thickness of 2.5 mm (i.e., eight plies), see actual micrograph inserts in Figure 4 (compliments of P. Bonacuse, NASA Glenn). The properties and necessary material parameters are listed in Table 1 to Table 3, wherein the elastic properties were determined from either published values or discussions with colleagues while the strength and damage parameters were obtain from correlation with the macrolevel tensile response curve, shown in Figure 11.

TABLE 1.—FIBER PROPERTIES

	Modulus (GPa)	Poisson's Ratio	Axial strength, GPa	Shear strength, MPa	σ_{dam} , MPa	n
iBN-Sylramic	400	0.2	2.2	900	---	----
CVI-SiC	420	0.2	---	---	180	0.04
Boron nitride	22	0.22	---	---	---	----

TABLE 2.—WEAVE PROPERTIES

Type.....	5HS
Fiber volume fraction	36%
Tow volume fraction.....	78%
Tow width.....	1.25 mm
Tow spacing.....	0.34 mm
Total Thickness.....	2.5 mm
Matrix	CVI-SiC

TABLE 3.—TOW PROPERTIES

Tow fiber volume fraction	46%
Tow packing structure	Square
Fiber.....	iBN-Sylramic
Matrix	CVI-SiC
Interface	BN

Typical Results

A typical response curve of an experimental, on-axis, tensile test is shown in Figure 11, taken from Morscher (see Refs. 8 and 9), and is overlaid with a baseline correlation using the localized void model (see Figure 7(c)). The simulated response shows good correlation with the experimental curve, approximately capturing the deviation from proportionality (often referred to as “first matrix cracking”) and failure stress. In Figure 12, the underlying mechanisms causing nonlinearity (which are subtle in some places), are denoted; the four primary events being: intra-tow matrix damage, inter-weave matrix damage (in the low void and also in the high void region) and then ultimate fiber failure. The multiple damage initiation points are due to two reasons. First, different regions of the weave RUC will initiate damage at different times. Secondly, different tow subcells within a given region initiate local damage at different time’s thus providing variable effective tow properties. It is useful also to look at the instantaneous secant elastic modulus, which degrades due to matrix damage as shown in Figure 13. It is easier to understand the degradation effects due to the matrix by directly looking at the stiffness effects. In a typical tensile response curve, there are four significant events that are useful for characterizing the material; these are: 1) initial modulus 2) point of deviation from linearity (often referred to as first matrix cracking or proportional limit stress (PLS)) 3) post first matrix cracking (i.e., damaged) modulus and 4) fiber failure point. The subsequent parametric study will focus on the impact that material and architectural parameters have on these four significant measures.

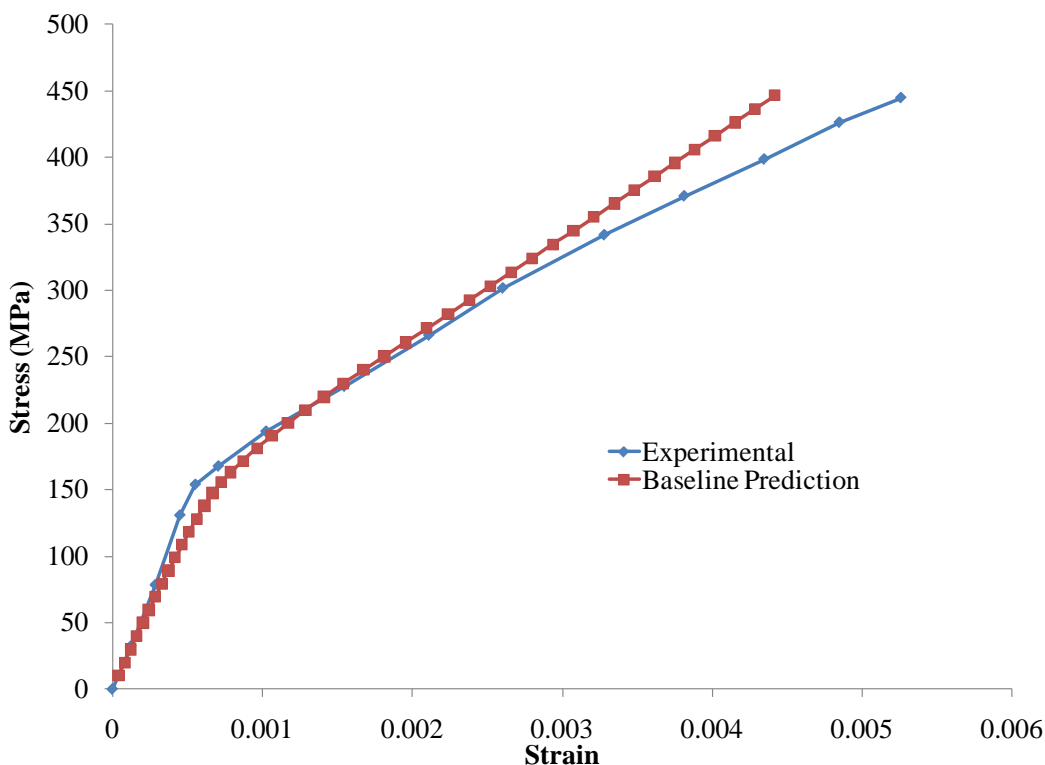


Figure 11.—Typical experimental response curve (Refs. 8 and 9).

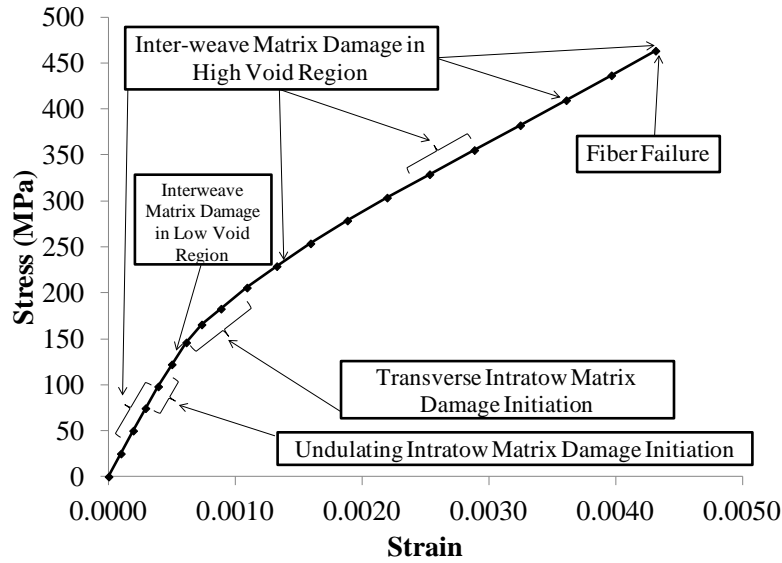


Figure 12.—Typical simulated response curve.

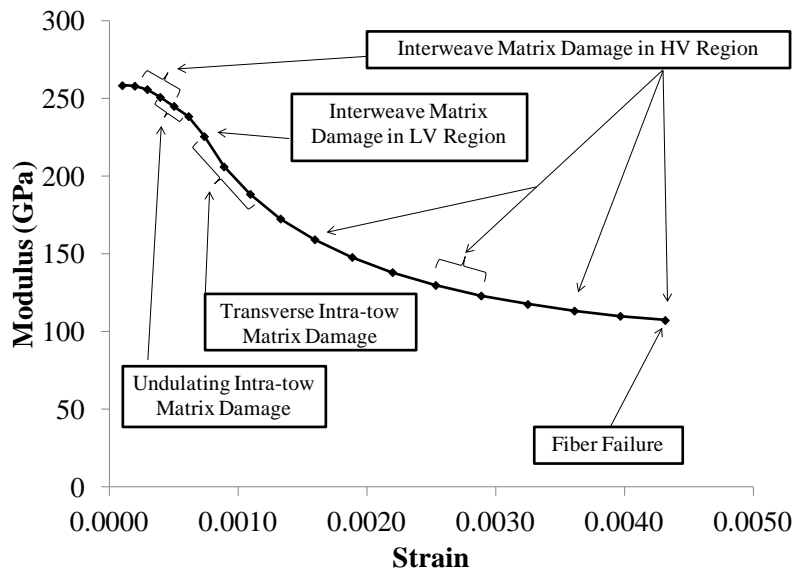


Figure 13.—Typical simulated secant modulus.

Furthermore, it is critical to understand the underlying mechanisms governing these events. In the case of the initial modulus, it is clear that the individual constituents' stiffness matrices and the weave architecture are primary drivers, along with possible microcracking of the matrix constituent. The fact that some damage occurs before the first major point of nonlinearity, is substantiated by the experimental acoustic emission results in Reference 8. Similarly, the model attributes this initial cracking to damage in the intra-tow matrix (undulating tow and transverse to the tow) and to damage in the high void density region of the inter-weave matrix (known as the high stressed region). The second event (i.e., the first major point of deviation from linearity) occurs at approximately 0.075 percent strain, for the CMC examined, is said to be "first matrix cracking". This point is taken to reflect a significant crack (or coalescence of microcracking) occurring in either the tow or weave matrix; thus enabling environmental attack of the composite. Correlating model results to that of the typical response (see Figure 7), the model predicts that cracking occurs in both the tow and weave, at "first matrix cracking". Thirdly, the slope of the post first matrix cracking curve (damage modulus) is determined by the response of the tows in the

loading direction, matrix material (i.e., the behavior after damage initiation) and corresponding constitutive model and weave architecture. Again, the experimental acoustic emission results (Ref. 7) are consistent with this in that they show some damage gradually occurring after first matrix cracking within this region of the response curve. This is most likely a combination of all previous damage growing as well as the onset of new damage in the high stressed regions. This damage progression continues with continuous local stress redistribution from matrix to tow/fiber until the final failure point is determined by reaching the failure strength of the fibers (in the applied load direction) within the tows. Note, although not considered here, MSGMC can incorporate statistical fiber breakage by modeling multiple fibers within the Tow RUC. Further although both the axial and shear fiber failure strength values given in Table 1, were backed out from the composite level tensile curve, these parameters should be experimentally determined from either individual monofilament and/or tow testing. To the authors knowledge such tests have not been conducted to date, but will be critical tests that should be done in the future.

Effects of Material Properties

To understand the influence of constituent material variation on the overall macro response; three of the matrix material constitutive model parameters (i.e., the initial modulus, post first matrix cracking modulus, n , and critical cracking stress, σ_{dam}) were varied. Note, these properties were varied a significant amount from the baseline so that their effect could be clearly seen. For example, the initial modulus was increased by 50 percent, in another case n was increased by 200 percent and in a third case σ_{dam} was increased by 100 percent; while holding all other properties at the baseline. Considering the results in Figure 11, one would expect that changing the matrix modulus should correspond to changing the initial weave modulus and post first matrix cracking modulus. This is in agreement with the results shown in Figure 14. In addition to the weave stiffness changing, the onset of “first matrix cracking” is also affected; resulting in a higher stress level (approximately 10 percent) and lower strain to failure (approximately 10 percent). Next changing only the parameter n from that of the baseline, one would expect the post first matrix cracking modulus to be primarily impacted, as verified in Figure 14, with a corresponding change in failure stress (e.g., increased 10 percent), failure strain (e.g., decreased 12 percent), and post secondary modulus (e.g., increased 120 percent). Finally, increasing σ_{dam} caused the “first matrix cracking” onset to be delayed (approximately 110 MPa, or 94 percent) resulting in higher overall failure stresses (increase of 8 percent) and a lower failure strain level of 0.0031 (a 24 percent reduction). Note that the initial weave modulus and post first matrix cracking modulus are nearly unchanged, in this case.

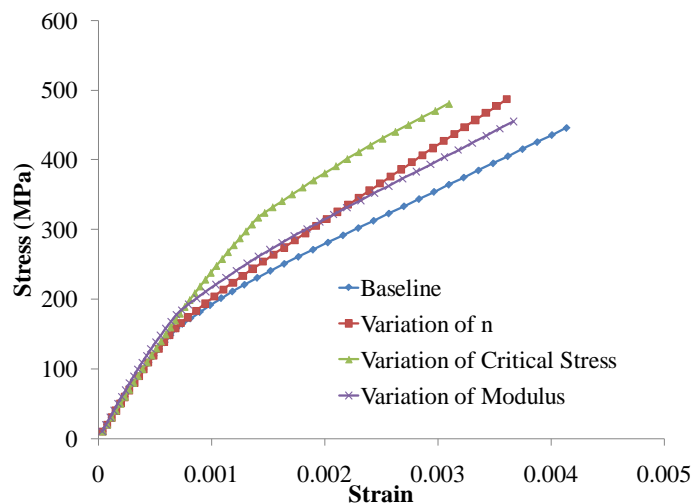


Figure 14.—Variation of matrix constituent material properties.

Effects of Architecture

To study the effects of architectural variation on the macroscale response, a full factorial set of numerical simulations were conducted. The parameters varied are shown in Table 4 and depicted in Figure 4. The three tow architectural parameters varied were: a) tow fiber volume fraction, b) tow aspect ratio, and c) tow void volume fraction. In addition, three weave void location cases were examined to illustrate the influence of void location due to manufacturing as well. All other parameters in the analysis were kept constant. Additionally, other architectural effects exist that the authors did not investigate which could possibly have an effect. These include inter-ply nesting, fiber packing structure, coating thickness, and fiber tow shifting to name a few. Future work will determine which of these parameters are the most significant. The tow fiber volume fraction and void volume fraction are both considered a mesoscale effect because their geometrical properties are involved in the mesoscale concentration matrix (Eq. (2)); whereas, the tow aspect ratio is considered a macroscale property because it is taken into account in the macroscale concentration matrices (Eqs. (5) and (11)). The tow volume was varied over a narrow range indicative of typical experimental variation: 0.46, 0.48, and 0.50. These three values were chosen based on common experimental values obtained for CMCs. Similarly, realistic tow aspect ratios were also chosen, i.e., 8, 10 and 12, where a value of 10 is typical for CMCs and three different fiber void volume fractions were used; 0.01, 0.05, and 0.07.

TABLE 4.—VARIED PARAMETERS

Architectural parameter	Relevant length scale	Values
Tow fiber volume fraction (V_f)	Meso	0.46,0.48,0.50
Tow void volume fraction	Meso	0.01,0.05,0.07
Tow aspect ratio (AR)	Macro	8,10,12
Weave void distribution	Macro	None, even, localized

In Figure 15 the effects of weave void distribution are examined; wherein three line plots (each corresponding to an assumed void distribution discussed earlier). Two cases, that is no void modeling and uniformly distributed voids, fail to capture the correct overall response. As the initial modulus is too stiff, “first matrix cracking” stress and failure stress levels are too high and the strain to failure too large. This is a result of incorrect local failure modes and local stress distribution. Therefore one can conclude that to accurately capture the overall in-plane deformation and failure response the analysis must incorporate accurate localized void distributions. In addition it has been observed (see Refs. 9 to 10) that the out-of-plane moduli is significantly reduced as compared to that calculated when void shape is not accurately accounted for; only recently, has a sheet like network of voids been microscopically observed, Bonacuse et al. (Refs. 11 and 12). Consequently, the influence of void shape is illustrated in Figure 16, wherein a cubic, cylindrical and sheet like void shape is examined given the case of localized voids. The out-of-plane moduli is significantly influenced by the assumed void shape, in that $E_z = 165, 172.5, \text{ and } 88.8 \text{ GPa}$, when one considers cubic, cylindrical and flat (or sheet like) voids, respectively. However, the in-plane response (both deformation and failure) is unaffected by void shape as shown in Figure 16, as one might expect.

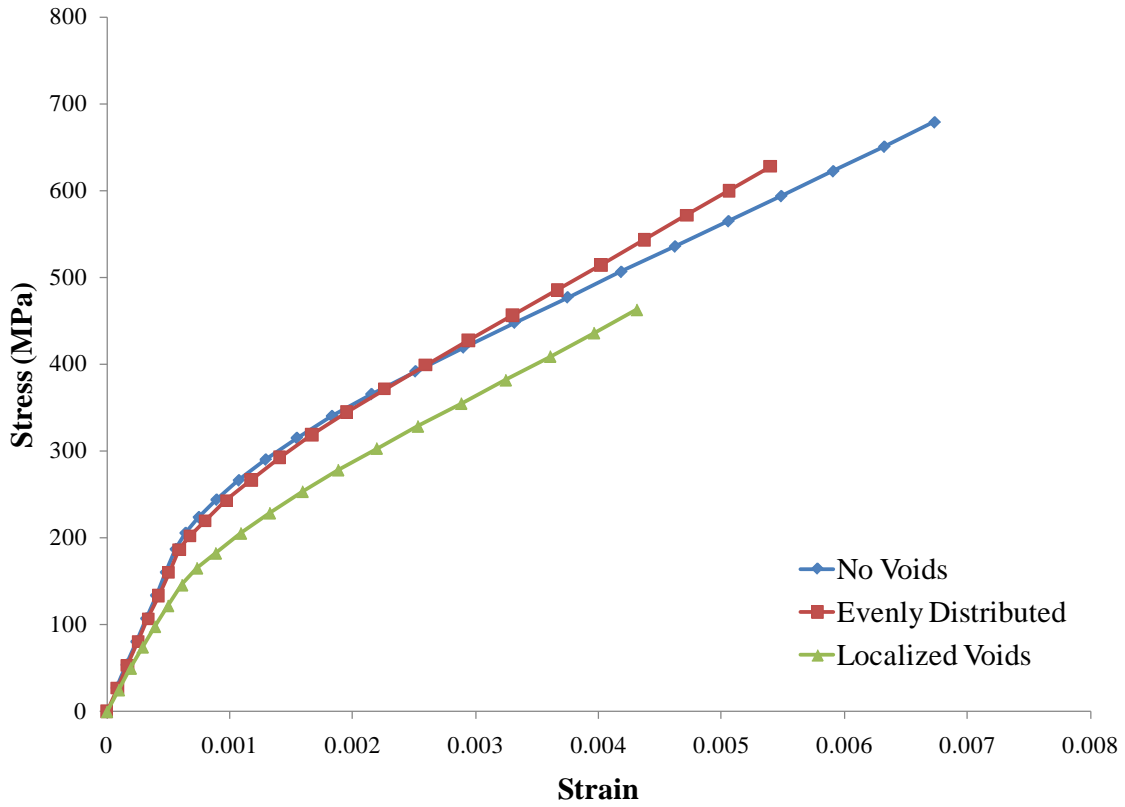


Figure 15.—Effects of weave void distribution.

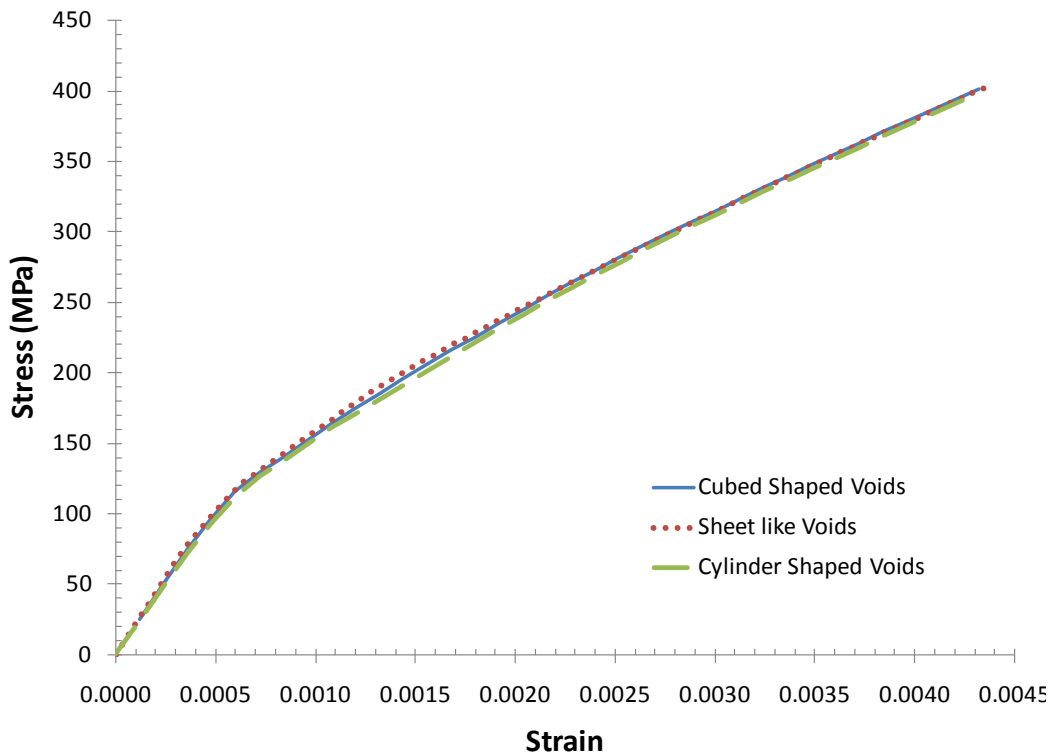


Figure 16.—Effect of void shape on tensile response, given localized void distribution.

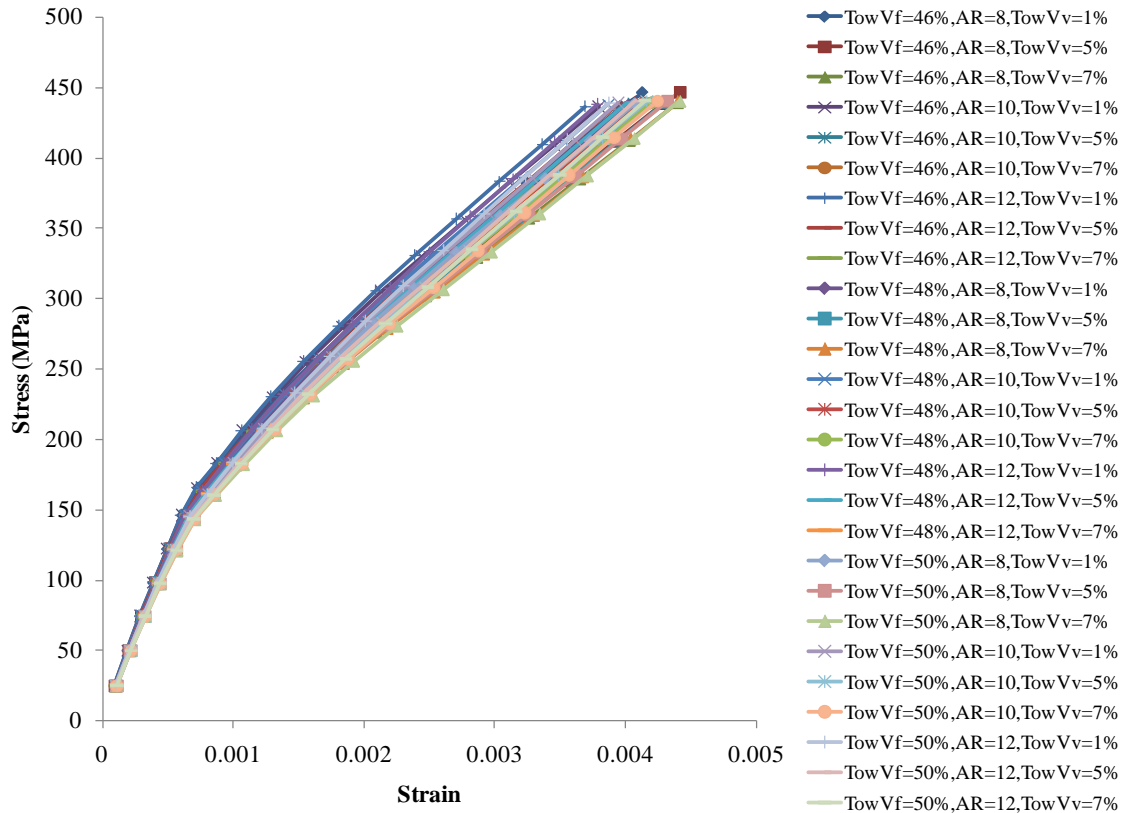


Figure 17.—All simulated cases.

The remaining parametric cases were all computed using the localized void model. However, it is important to note that the tow fiber volume fraction and weave void volume fraction are coupled and cannot be decoupled within the analysis, since when the fiber volume fraction within the tow increases, the tow spacing must increase in order to maintain continuity of the overall fiber volume fraction and thickness. This therefore creates a large volume domain for voids to fill, thus increasing the overall void content. Correspondingly, the effect of increasing void content and tow volume fraction are coupled together. The total variation in stress–strain response for all cases are shown in Figure 17. Clearly, the overall response characteristic is very similar, irrespective of the value of the individual parameters, with the variation in the initial modulus being at most 22 percent, first matrix cracking approximately 16 percent and the ultimate tensile stress (UTS) for all practical purposes being identical. Furthermore, the post first matrix cracking modulus changes some 24 percent (i.e., from 72 to 90 GPa) with a corresponding 16 percent change in final failure strain. The configuration providing the stiffest response is composed of a tow volume fraction of 46 percent, aspect ratio (AR) equal to 12 and tow void fraction of 1 percent, whereas the most compliant response is generated using a tow volume fraction of 50 percent, aspect ratio (AR) equal to 8 and tow void fraction of 7 percent.

In Figure 17 through Figure 20 the various responses are arranged so as to enable identification of parameter sensitivities. Figure 18 shows the effect of tow void content on the overall response; where it can be seen that increasing the void content within the tow (thus lowering its effective stiffness) causes the macro response curve to be more compliant with generally an effect of increasing the strain to failure. Figure 19 shows the effect of tow aspect ratio; where increasing the aspect ratio has the effect of stiffening the response curve and lowering the failure stress. Figure 20 displays the influence of tow fiber volume fraction, which appears to be minimal at first glance. Although this trend is possible, as mentioned previously, it is strongly coupled with the overall weave void volume fraction and thus these

two effects could be working in opposition to one another. Consequently, it is impossible to deduce from these graphs, the overall effect of tow fiber volume fraction.

Comparing all parameters, the weave void locations, tow void content, fiber volume fraction within a tow and tow aspect ratio, one can assess the severity of these effects. For example, it is clear from Figure 15, that the location (and shape) of voids at the macroscale is a critical driving parameter relative to failure. This far outweighs all other parameters. Similarly, the effect of inter-ply tow nesting could also be a critical/primary driving factor, yet this effect has been left for future work. Besides the weave void content (i.e., location and shape), the tow void content has the strongest effect on post first matrix cracking stiffness and the tow aspect ratio has the strongest effect on failure strain. The tow fiber volume fraction appears to have a minimal effect relative to other parameters.

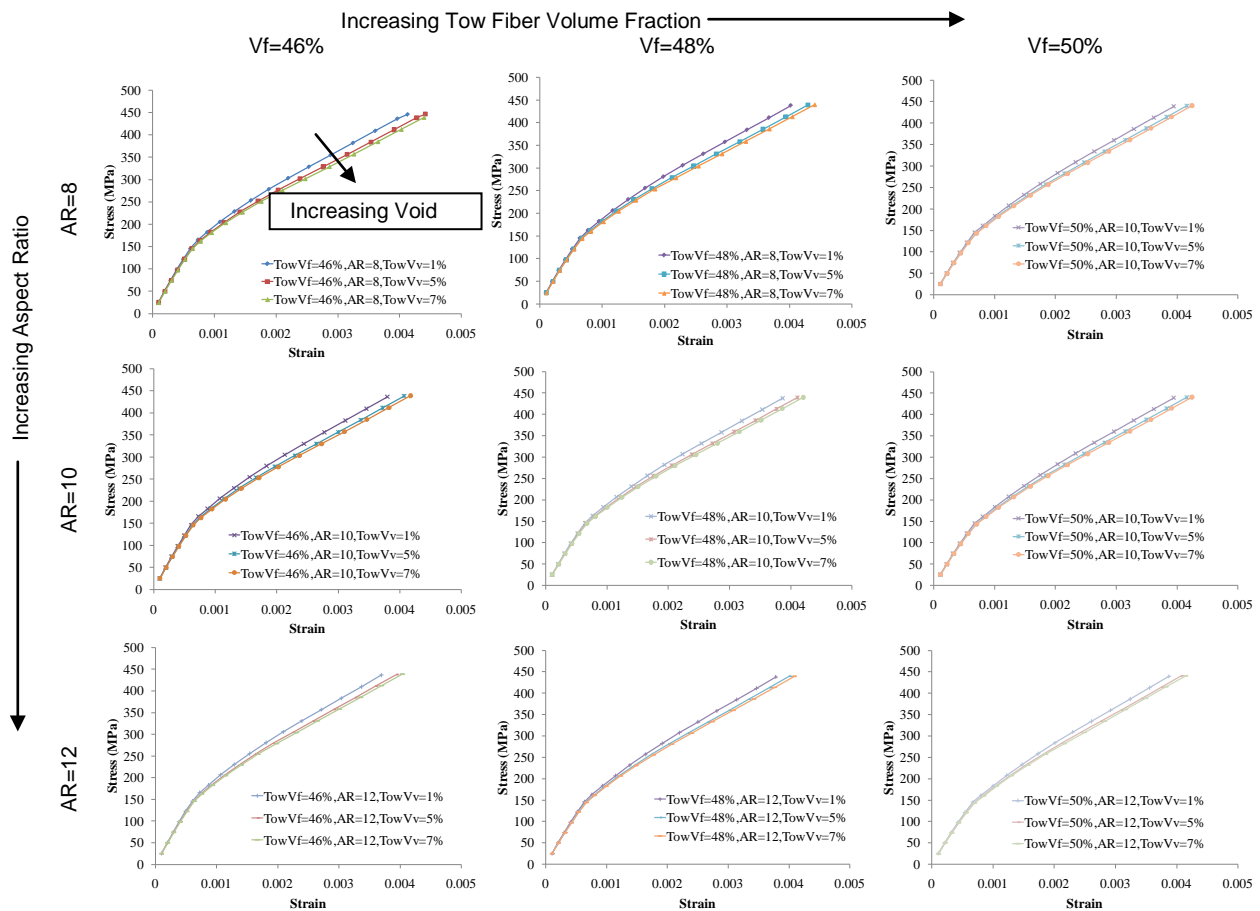


Figure 18.—Effects of tow void content.

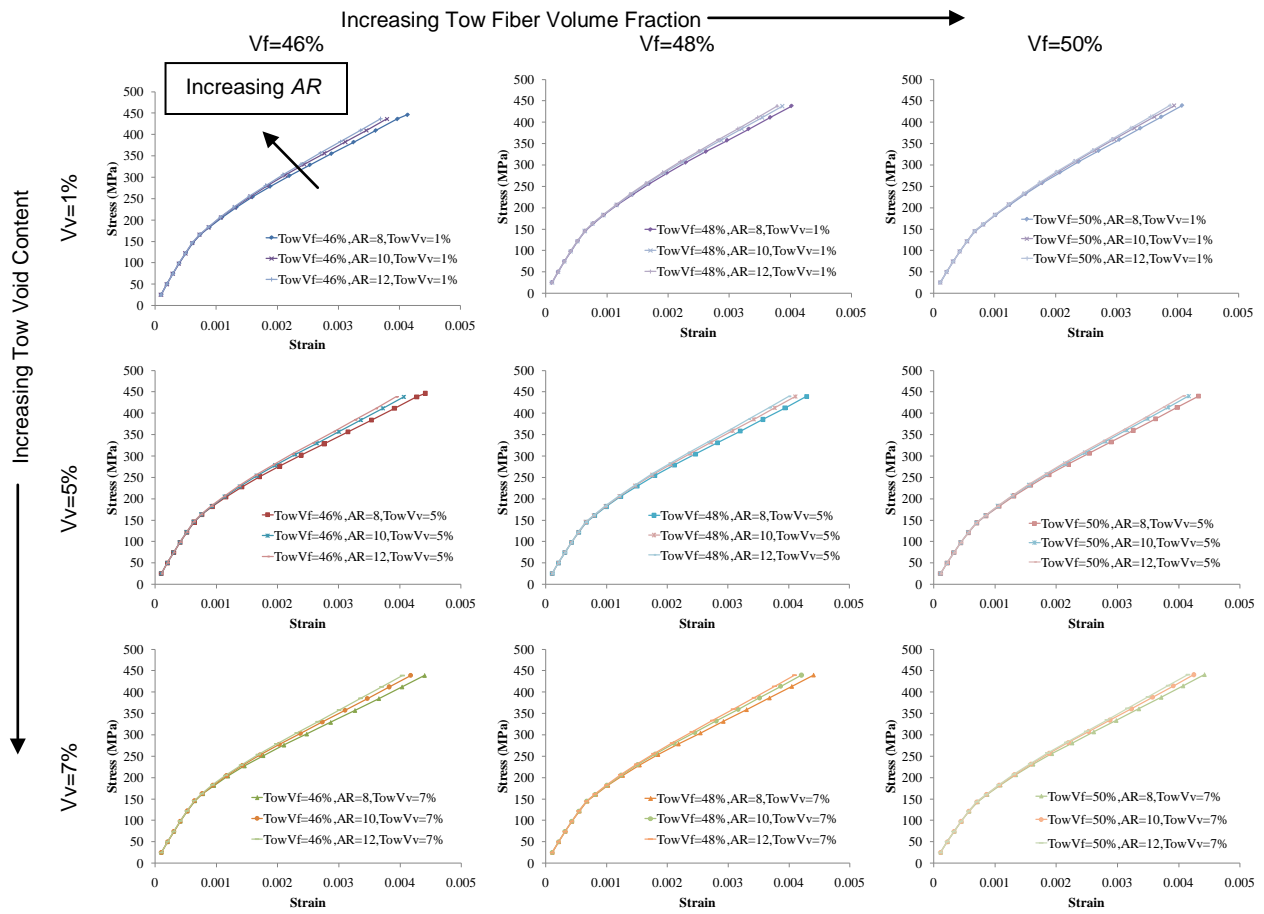


Figure 19.—Effects of aspect ratio.

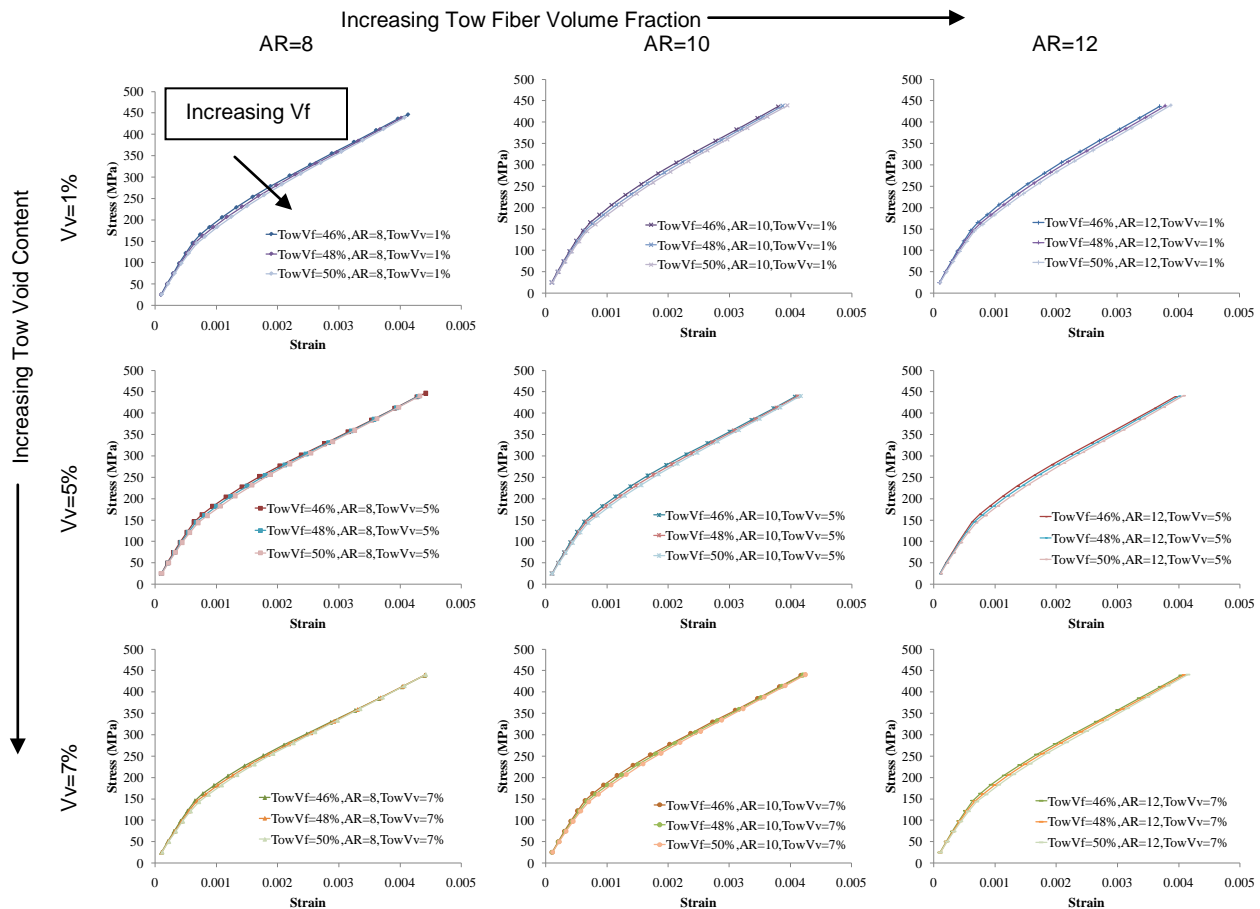


Figure 20.—Effects of tow volume fraction.

Conclusion

This paper presents a detailed investigation into several architectural and material parameter effects on the macroscale deformation response of a five harness satin (5HS) woven CMC. The recently implemented Multiscale Generalized Method of Cells (MSGMC) methodology was employed to model the nonlinear damage driven response of a 5HS woven composite fabric, where four separate material scales were considered. At the microscale, the influence of constituent material properties was investigated. At the mesoscale, the tow fiber volume fraction and the void content within a tow were varied; whereas at the macroscale the influence of the tow aspect ratio and weave void content were investigated. For each permutation of these effects, the tensile response to failure was analyzed; wherein the modulus, first matrix cracking, post damage modulus, and ultimate failure strain were examined. Analyzing the macroscale response, it was determined that the location of the weave void content at the macroscale was the most impactful parameter for capturing failure related properties (PLS and UTS). It is critical that this effect be captured and correctly reflected in a model to ensure accurate deformation and failure response. Further, the void shape should be idealized as a flat sheet in order to obtain accurate out-of-plane stiffness predictions. Secondly, tow void content had the largest effect on the initial and post stiffness with the tow aspect ratio greatly influencing the failure strain levels. Also, it appears that accurately modeling inter-tow failure is critical to predicting the deviation from proportionality. Finally, structural scale analysis parameter sensitivity along with tow/weave irregularities will be a topic of future work.

References

1. Liu, K. and Chattopahdyay, A. and Bednarczyk, B. and Arnold, S.M.: “Efficient Multiscale Modeling Framework For Triaxially Braided Composites using Generalized Method of Cells,” *Journal of Aerospace Engineering*, April 2011.
2. Paley, M. and Aboudi, J.: “Micromechanical Analysis of Composites by the Generalized Method of Cells,” *Mechanics of Materials* 1992; 14: 127–139.
3. Aboudi, J.: “Micromechanical Analysis of Thermo-Inelastic Multiphase Short-Fiber Composites”, *Composite Eng.* **5**, 839-850, 1995.
4. Liu, K.C., Arnold, S.M., Chattopadhyay, A.; “Examination of Material and Architectural Effects at Various Length Scales on the Structural Deformation Response of Woven Polymeric Composites Determined Via Multiscale Generalized Method of Cells, 51st AIAA/ASME/ASCE/AHS/ACS Structures, Structural Dynamics, Materials Conference, Orlando, FL (April 12-15, 2010).
5. Bednarczyk, B.A.: “Modeling Woven Polymer Matrix Composites With MAC/GMC,” NASA/CR—2000-210370.
6. Liu, K.C., Hiche, C. and Chattopadhyay, A.: “Low Speed Projectile Impact Damage Prediction and Propagation in Woven Composites,” 50th AIAA/ASME/ASCE/AHS/ASC Structures, Proc. Structural Dynamics and Materials Conference, Palm Springs, CA, May 2009.
7. Hashin, Z.: “Failure Criteria for Unidirectional Fiber Composites,” *J. Appl. Mech.*, Vol. 47, June 1980, pp. 329–334.
8. Morscher, G.: “Stress, matrix cracking, temperature, environment, and life of SiC/SiC woven composites” International Conference on High Temperature Ceramic Matrix Composites, Bayreuth, Germany, Sep. 20–22, 2010.
9. Morscher, G. N., Singh, M., Kiser, J.D., Freedman, M., and Bhatt, R.: “Modeling stress-dependent matrix cracking and stress-strain behavior in 2D woven SiC fiber reinforced CVI SiC composites,” *Composites Science and Technology*, Vol. 67, 2007, pp. 1009–1017.
10. Mital, S., Bednarczyk, B.A., Arnold, S.M., and Lang, J.; “Modeling of Melt-Infiltrated SiC/SiC Composite Properties”, NASA/TM—2009-215806.
11. Bonacuse, P.J., Mital, S., and Goldberg, R.; “Characterization of the As Manufactured Variability in a CVI SiC/SiC Woven Composite”, GT2011-45890, Proceedings of ASME Turbo Expo 2011, June, Vancouver, Canada, 2011.
12. Bonacuse, P.J., private communications, 2011.

REPORT DOCUMENTATION PAGE			Form Approved OMB No. 0704-0188	
<p>The public reporting burden for this collection of information is estimated to average 1 hour per response, including the time for reviewing instructions, searching existing data sources, gathering and maintaining the data needed, and completing and reviewing the collection of information. Send comments regarding this burden estimate or any other aspect of this collection of information, including suggestions for reducing this burden, to Department of Defense, Washington Headquarters Services, Directorate for Information Operations and Reports (0704-0188), 1215 Jefferson Davis Highway, Suite 1204, Arlington, VA 22202-4302. Respondents should be aware that notwithstanding any other provision of law, no person shall be subject to any penalty for failing to comply with a collection of information if it does not display a currently valid OMB control number.</p> <p>PLEASE DO NOT RETURN YOUR FORM TO THE ABOVE ADDRESS.</p>				
1. REPORT DATE (DD-MM-YYYY) 01-11-2011		2. REPORT TYPE Technical Memorandum		3. DATES COVERED (From - To)
4. TITLE AND SUBTITLE Impact of Material and Architecture Model Parameters on the Failure of Woven Ceramic Matrix Composites (CMCs) Via the Multiscale Generalized Method of Cells			5a. CONTRACT NUMBER	
			5b. GRANT NUMBER	
			5c. PROGRAM ELEMENT NUMBER	
6. AUTHOR(S) Liu, Kuang, C.; Arnold, Steven, M.			5d. PROJECT NUMBER	
			5e. TASK NUMBER	
			5f. WORK UNIT NUMBER WBS 031102.02.02.03.0249.11	
7. PERFORMING ORGANIZATION NAME(S) AND ADDRESS(ES) National Aeronautics and Space Administration John H. Glenn Research Center at Lewis Field Cleveland, Ohio 44135-3191			8. PERFORMING ORGANIZATION REPORT NUMBER E-17674	
9. SPONSORING/MONITORING AGENCY NAME(S) AND ADDRESS(ES) National Aeronautics and Space Administration Washington, DC 20546-0001			10. SPONSORING/MONITOR'S ACRONYM(S) NASA	
			11. SPONSORING/MONITORING REPORT NUMBER NASA/TM-2011-217011	
12. DISTRIBUTION/AVAILABILITY STATEMENT Unclassified-Unlimited Subject Categories: 24 and 39 Available electronically at http://www.sti.nasa.gov This publication is available from the NASA Center for AeroSpace Information, 443-757-5802				
13. SUPPLEMENTARY NOTES				
14. ABSTRACT It is well known that failure of a material is a locally driven event. In the case of ceramic matrix composites (CMCs), significant variations in the microstructure of the composite exist and their significance on both deformation and life response need to be assessed. Examples of these variations include changes in the fiber tow shape, tow shifting/nesting and voids within and between tows. In the present work, the effects of many of these architectural parameters and material scatter of woven ceramic composite properties at the macroscale (woven RUC) will be studied to assess their sensitivity. The recently developed Multiscale Generalized Method of Cells methodology is used to determine the overall deformation response, proportional elastic limit (first matrix cracking), and failure under tensile loading conditions. The macroscale responses investigated illustrate the effect of architectural and material parameters on a single RUC representing a five harness satin weave fabric. Results shows that the most critical architectural parameter is weave void shape and content with other parameters being less in severity. Variation of the matrix material properties was also studied to illustrate the influence of the material variability on the overall features of the composite stress-strain response.				
15. SUBJECT TERMS Polymer matrix composites; Braided composites; Finite element method; Micromechanics				
16. SECURITY CLASSIFICATION OF:			17. LIMITATION OF ABSTRACT UU	18. NUMBER OF PAGES 28
a. REPORT U	b. ABSTRACT U	c. THIS PAGE U		
			19b. TELEPHONE NUMBER (include area code) 443-757-5802	

